Tumor cell plasticity, heterogeneity and resistance in crucial microenvironmental niches in glioma

Erik Jung
German Cancer Research Center (DKFZ)
Matthias Osswald
University Hospital Heidelberg
Miriam Ratliff
German Cancer Research Center
Ruifan Xie
German Cancer Research Center
Sophie Weil
University Hospital Heidelberg
Felix Kurz
Department of Neuroradiology, University Hospital of Heidelberg, Heidelberg
Felix Sahm
Institute of Pathology, University Hospital Heidelberg and Clinical Cooperation Unit Neuropathology, German Cancer Research Center (DKFZ) https://orcid.org/0000-0001-5441-1962
Andreas von Deimling
University Hospital Heidelberg
Sabine Heiland
University Hospital Heidelberg
Wolfgang Wick
Heidelberg University https://orcid.org/0000-0002-6171-634X
Frank Winkler (frank.winkler@med.uni-heidelberg.de)
University Hospital Heidelberg https://orcid.org/0000-0003-4892-6104

Article

Keywords: glioblastoma, perivascular niche, tumor microtubes, resistance to therapy, tumor cells

Posted Date: July 10th, 2020

DOI: https://doi.org/10.21203/rs.3.rs-39208/v1

Version of Record: A version of this preprint was published at Nature Communications on February 12th, 2021. See the published version at https://doi.org/10.1038/s41467-021-21117-3.

Abstract

Both the perivascular niche (PVN) and the integration into multicellular networks by tumor microtubes (TMs) have been associated with progression and resistance to therapies in glioblastoma, but their specific contribution remained unknown. By long-term tracking of tumor cell fate and dynamics in the live mouse brain, differential therapeutic responses in both niches could be determined. Both the PVN, a preferential location of long-term quiescent glioma cells, and network integration facilitated resistance against cytotoxic effects of radiotherapy and chemotherapy - independently of each other, but with additive effects. Perivascular glioblastoma cells were particularly able to actively repair damage to tumor regions. Population of the PVN and resistance in it depended on proficient NOTCH1 expression. In turn, NOTCH1 downregulation induced resistant multicellular networks by TM extension. Our findings identify NOTCH1 as a central switch between the PVN and network niche in glioma, and demonstrate robust cross-compensation when only one niche is targeted.

Introduction

Malignant gliomas, including glioblastoma, are the most frequent and yet incurable primary brain tumors characterized by early infiltrative growth and high therapy resistance [1]. Apart from frank angiogenesis, the vasculature of the brain and the tumor seems to play a special role in glioma biology: a subpopulation of stem-like cells was identified in brain tumors that is potentially responsible for their frequent treatment failure [2, 3, 4, 5], and these stem-like cells can inhabit distinct perivascular niches (PVN) [6, 7, 8, 9, 10]. Importantly, those stem-like glioma cells share marker expression and molecular traits with neural stem cells (NSCs) [2, 3], and NSCs also populate distinct neurogenic niches, which include PVN that provide a unique microenvironment for the preservation of the stem cell pool [11]. Targeting of the PVN thus emerged as a novel strategy to eradicate cancer stem-like cells in incurable gliomas, to improve their response to therapy response and to prevent tumor recurrence [9, 12], but at the same time raised the question of the collateral effects associated with it.

In line with the neurodevelopmental origins of glioma [13, 14] and shared traits between neural progenitor cells and glioma cells, neurite-like cellular protrusions named tumor microtubes (TMs) have recently been characterized in gliomas [15, 16]. TMs are leading structures during glioma cell invasion [15, 17] and enable glioma cells to form functional, communicating multicellular networks that render network members resistant against cytotoxic therapies, likely due to improved cellular homeostasis [15, 18].

All in all, while there is increasing evidence that interactions with pre-existing blood vessels in the brain are of importance for tumor progression and resistance in glioma, their exact cellular and molecular mechanisms and overall role in brain tumor biology are not sufficiently understood. By following patient-derived primary glioblastoma cells dynamically for extended periods of time with *in vivo* two photon microscopy, we here describe novel mechanisms of tumor progression that depend on interactions with brain microvessels and tumor cell networks, and provide the first definitive confirmation that the *NOTCH1*-

dependent PVN is a primary niche of resistance in brain tumors. We also demonstrate that *NOTCH1* is an important modulator of TM-network formation, and interference with this pathway leads to a partial cross-compensation between these two prime niches of resistance in glioma.

Results

A perivascular niche for long-term quiescent glioblastoma cells

First, we asked how tumor cells in patient samples from diffusely infiltrating gliomas are distributed in relation to blood vessels in the brain. Mutation-specific immunohistochemical stainings against IDH1-R132H were used, which allows specific detection of tumor cell structures vs. nonmalignant brain cells in human glioma samples [19, 20]. In these specimens, a minority of tumor cells closely associated with blood vessels in a distinct perivascular niche (Fig. 1A, B), a phenotype that could also be recapitulated in a patient-derived xenograft model growing in the mouse brain (Fig. 1C). In both human (Fig. 1D,E) and mouse (Fig. 1F) tumor samples, the majority of tumor cells populated the parenchymal compartment distant from blood vessels (Fig. 1A,D-F). Of note, many parenchymal but also some perivascular cells were clearly characterized by the extension of TMs (Fig. 1B-F) which connected single glioma cells to a network of tumor cells, as described before [15, 21, 22]. This TM-connected tumor cell network becomes most evident in 3D reconstructions of thick sections from man (Fig. 1D) and mouse (Fig. 1F).

The study of individual glioblastoma cells in these two niches - their plasticity, heterogeneity, stroma interactions, contribution to tumor progression, and their response to therapies – would greatly benefit from the ability to dynamically long-term track individual tumor cells [23]. Thus, to investigate the relative impact and dynamic interplay of the PVN and TM network niches, we used a mouse xenograft models that closely reflect the growth pattern of malignant gliomas in humans, combined with intravital two photon-microscopy that allows to follow tumor microregions over long periods (up to months) in the three-dimensional space of the brain in living mice [15, 17, 18, 21]. By long-term tracking of glioma cells in invasive tumor regions (Fig. 2A), we identified a subset of tumor cells that did not change their position over days to weeks, although being located at the invasive front. A significant majority of those long-term quiescent cells were found in a strict perivascular niche (PVN) position (Fig. 2B), closely following the course of blood vessels by stretching out to an elongated shape. A fluorescent reporter for tumor cell nuclei allowed to follow mitotic events in those cells. Here, the adjacent daughter cells remained closely associated with respective blood vessel after cell division (Fig. 2C).

In the tumor core which is characterized by a higher cellular density and dense TM-connected tumor cell networks (Fig. 2A), the majority of PVN cells remained resident over weeks, whereas many parenchymal cells were still migrating (Fig. 2D). Histological analyses revealed that perivascular cell clusters were located between astrocytic endfeet and endothelial cells of brain microvessels (Fig. 2E), thus integrating into structures of the blood-brain barrier. Although the tumor cell soma remained at the very same spot

over weeks, these perivascular cells actively extended and retracted TMs, scanning the environment and transiently or permanently connecting with neighboring cells (Fig. 2F). Some resident cells were closely associated with remodeled vessels such as capillary loops or glomeruloid-like bodies (Fig. 2G), but the majority colonized morphologically unaltered vessels.

Histological analyses revealed that the proliferation rate of perivascular cells was lower compared to parenchymal cells (Fig. 3A). As cell bodies and TMs of perivascular cells often stretch out into the parenchymal compartment, intravital microscopy was used to analyze cell and vessel associations in larger 3D volumes. This analysis confirmed that the normalized mitotic rate of perivascular cells was lower compared to the parenchymal subpopulation (Fig. 3B). In summary, perivascular cells constitute a major fraction of long-term resident glioblastoma cells, both at the invasive front and in the established tumor core, and are characterized by a quiescent state.

The perivascular localization is associated with tumor cell resilience

In neurogenic niches and brain tumors alike, the PVN provides a specific microenvironment for stem-like cells, which has been linked to cellular resilience [6, 7, 12, 24]. Furthermore, our group recently characterized the integration of glioma cells into TM-connected multicellular networks as a novel mechanism of resistance to cytotoxic therapies and prerequisite for tumor self-repair [15, 18]. This leads to the question of the interrelation and relative relevance of both key factors of glioma progression and tumor cell persistence. More cells in the parenchymal compartment extended 2 TMs (Fig. 4A), a phenotype associated with fast invasion [17]. Moreover, a significant fraction of cells without any TMs was only found in the perivascular compartment (Fig. 4A). The degree of integration into multicellular networks did not appear to be relevantly biologically different between parenchymal and perivascular tumor cells (Fig. 4B).

After application of radiotherapy, PVN cells turned out to be highly radioresistant, whereas the number of parenchymal cells was significantly reduced by therapeutic irradiation as early as 7 days later (Fig. 4C). To rule out that the higher resistance of PVN cells was due to their sole integration into the tumor network, a subgroup analysis was performed. This analysis revealed that both non-connected and connected perivascular tumor cells resisted the cytotoxic effects of radiotherapy, whereas non-connected cells in the parenchyma responded well to radiotherapy (Fig. 4D). Integration into tumor cell networks conveyed additive effects in the PVN (Fig. 4D).

Likewise, after temozolomide (TMZ) chemotherapy, a higher resistance of perivascular glioblastoma cells was confirmed in the S24 GBMSC line, and again this resistance could not be explained by differential tumor cell connectivity, at least not solely (Fig. 4E). In T269 gliomas derived from another MGMT promoter hypermethylated GBMSC line which is more sensitive to chemotherapy than S24 and also more quickly proliferating *in vivo* [18], perivascular glioblastoma cells also resisted TMZ better than parenchymal ones (Fig. 4F).

After surgery and also after targeted ablation of one single tumor cell within the tumor cell network, a repair response with directed extension of newly formed TMs towards the lesion, replacement of network-integrated glioblastoma cells, and repopulation of the damaged tumor region has been described [18, 25]. We hence investigated whether perivascular and parenchymal tumor cells differed in their reactivity to a direct traumatic event. After inducing a microtrauma by ablation of one single glioblastoma cell with a high-power laser beam, an early reaction of a perivascular cell in this tumor microregion very frequently occurred within two hours, while parenchymal cells showed less reactivity (Fig. 4G). Of note, this early reaction was independent of the TM network connectivity of the ablated cell ($p = 0.119$, Fisher's exact test), thereby suggesting a paracrine rather than a network-mediated signal. Furthermore, after milder laser damage to a larger tumor area, a massive increase in tumor cell count in the damaged area was reproducibly inducible 4 days later, and this "malignant healing response" was strikingly accentuated in the PVN (Fig. 4H).

In summary, the perivascular localization of glioblastoma cells was associated with their therapy resistance and tumor cell resilience, additive to TM connectivity. Despite their static and often dormant behavior under resting conditions, perivascular cells can exhibit a strong reactivity to stress and damage.

PVN colonization and TM networks are inversely regulated by NOTCH1

Next we asked the question how both niches of resistance are molecularly interrelated: can glioblastoma cells dynamically change their position between the PVN and TM network niche, cross-compensating a molecular deficiency that deprives them of one or the other? For this we first inhibited network function by knockdown of the gap junction protein Cx43, which is a known connector of TM networks [15]. Here, morphological tumor cell networks greatly decreased, and tumor cells were driven into a perivascular position with high numbers of perivascular tumor cell clusters (Fig. 5A).

This led to the question whether a defect in PVN colonization in turn drives TM network integration of glioblastoma cells. Several publications suggested that activation of the *NOTCH1* pathway is associated with glioma cell properties in the PVN, including cellular stemness [7, 26, 27]. Interestingly, the *NOTCH1* pathway also plays an important role in neurite outgrowth [28], which shares many features with TM formation [15, 16, 17, 29]. Hence, we sought to elucidate its relevance for both the PVN and TM network niche. Immunohistological analyses demonstrated a *NOTCH1* pathway activation in perivascular tumor cells (Fig. 5B), confirming earlier results [7].

We next used shRNA mediated knockdown of *NOTCH1* to investigate the effects on brain and niche colonization as well as tumor cell morphology *in vivo*. Downregulation of *NOTCH1* expression led to decreased vascular co-option (Fig. 5C) and a reduction of the perivascular tumor cell population (Fig. 5D). On the other hand, TM formation was markedly induced, with longer TMs (Fig. 5E), an early shift to highly interconnected cellular subpopulation with more than 4 TMs (Fig. 5F), and the formation of dense multicellular networks (Fig. 5G,H).

Brain tumor cells integrated into multicellular networks and those remaining unconnected *in vivo* can be separated based on their differential uptake of the fluorescent dye SR101 [15, 21]. We separated both cell populations by FACS and performed RNA sequencing of bulk populations. Analyses of the differential expression in two primary glioblastoma cell lines (S24 and T269) confirmed downregulation of the *NOTCH1* receptor and of several genes associated with *NOTCH1* pathway activation in the connected tumor cell population, and also upregulation of genes associated with NOTCH1 pathway inhibition (Table 1).

Table 1
Interconnected tumor cells exhibit *NOTCH1* pathway downregulation

Bulk RNA sEq. of connected vs. non-connected tumor cells *in vivo*				
NOTCH1 **pathway activation**				
Gene	**log2 fold change (S24 GBMSCs)**	**adjusted p value (S24 GBMSCs)**	**log2 fold change (T269 GBMSCs)**	**adjusted p value (T269 GBMSCs)**
NOTCH1	-0.8411	0.0097	-0.6468	0.0122
HES6	-1.4296	6.2899e-6	-1.4490	5.4451e-8
DLL1	-2.3525	5.8021e-14	-2.6558	4.9849e-28
MFNG	-1.8398	1.018e-5	-2.8051	1.3372e-12
SATB1	-1.8029	1.8930e-6	-1.3847	1.9251e-8
MYCL	-1.2588	0.0016	-0.8474	0.0178
MYCN	-1.1416	0.0378	-1.0212	3.1898e-8
CDKN1C	-1.2697	0.0010	-2.3721	9.7218e-11
SOX8	-1.0591	1.3633e-4	-1.5615	4.3253e-27
ASCL1	-0.9464	0.0067	-1.1870	0.0081
PTPRJ	-0.8798	0.0350	-1.5500	0.0021
NOTCH1 **pathway inhibition**				
Gene	**log2 fold change (S24 GBMSCs)**	**adjusted p value (S24 GBMSCs)**	**log2 fold change (T269 GBMSCs)**	**adjusted p value (T269 GBMSCs)**
CDK1	0.8195	0.0076	1.2082	7.9934e-5
CHI3L1	1.1131	3.7427e-4	1.5617	2.5644e-6

Comparison of differential expression of genes associated with *NOTCH1* pathway activation and inhibition respectively between connected and non-connected S24 and T269 orthotopically xenografted glioblastoma cells. Connected and non-connected tumor cells were separated by FACS based on their uptake of SR101 *in vivo* before bulk RNA sEq. was performed. Only genes with significant differential expression as determined by an adjusted p-value < 0.05 are shown.

In contrast to glioblastomas, 1p/19q-codeleted oligodendrogliomas are characterized by sensitivity to cytotoxic therapies [30, 31] and network deficiency [15] (Fig. 6A). Compared to TM- and network proficient S24 glioblastoma cells, BT088 oligodendroglioma cells show a high *NOTCH1* expression (Fig. 6A). In addition, we reanalyzed and compared TCGA gene expression data of molecular glioblastomas vs. oligodendrogliomas [15] and found a relative downregulation of the *NOTCH1* gene and several downstream targets of the *NOTCH1* pathway, as well as an upregulation of genes associated with *NOTCH1* pathway inhibition in glioblastoma (Table 2). After shRNA-mediated knockdown of *NOTCH1*, BT088 oligodendroglioma cells were not able to give rise to tumors in immunodeficient mice as cells slowly regressed over time (Fig. 6B).

Table 2

The *NOTCH1* pathway is activated in human oligodendrogliomas compared to glioblastomas

Molecular human glioblastoma vs. molecular human oligodendroglioma				
NOTCH1 **pathway activation**				
Gene	**Entrez ID**	**log2 fold change**	**p value**	**FDR**
SOX8	30812	-2.5180613	5.39E-43	5.67E-41
DLL3	10683	-2.4262425	1.26E-17	1.33E-16
HEY1	23462	-1.2942635	9.18E-23	1.53E-21
MYC	4609	-1.2213157	3.76E-15	3.05E-14
HES6	55502	-1.1642784	1.29E-08	5.07E-08
DLL1	28514	-1.0985485	9.11E-08	3.25E-07
SATB1	6304	-0.8875692	5.68E-11	2.92E-10
ZMIZ1	57178	-0.8720752	7.95E-17	7.77E-16
NOTCH1	4851	-0.5352691	5.91E-05	0.00014523
CDKN1B	1027	-0.4286673	2.34E-09	1.00E-08
CCND1	595	-0.3288129	0.12248947	0.16628677
ASCL1	429	-0.2774871	0.1584482	0.20949394
CDKN1A	1026	-0.1732208	0.40000144	0.46701398
PTPRJ	5795	-0.1423327	0.20323507	0.26025615
JAG1	182	1.45417948	3.46E-21	4.94E-20
NOTCH1 **pathway inhibition**				
Gene	**Entrez ID**	**log2 fold change**	**p value**	**FDR**
CHI3L1	1116	5.41391741	2.64E-35	1.46E-33
NUMB	8650	0.6442456	1.12E-19	1,46E-18

Comparison of RNA expression data (TCGA) of molecular glioblastoma (n = 56) and molecular 1p/19q-codeleted oligodendroglioma (n = 70) reveals downregulation of genes associated with *NOTCH1* pathway activation in glioblastoma and upregulation of genes associated with *NOTCH1* pathway inhibition. FDR: False discovery rate.

NOTCH1 - dependent niche positions regulate growth and resistance in gliomas

To understand how these differential changes of tumor cell niche integrations after *NOTCH1* downregulation influence the overall sensitivity of gliomas to cytotoxic therapy, we analyzed tumor cell

responses to radiotherapy, and found it decreased for the total shNOTCH1 glioblastoma cell population (Fig. 7A). Deeper analysis revealed that this can exclusively be attributed to the increased radioresistance of the more abundantly TM-interconnected shNOTCH1 cells, whereas the fewer non-TM connected cells were even more vulnerable to radiotherapy in shNOTCH1 tumors (Fig. 7B). Further subgroup analysis revealed that this effect was due to an increased therapy response of the remaining non-connected perivascular cells (Fig. 7C), suggesting that *NOTCH1* proficiency is relevant for the resistance of perivascular cells to radiotherapy. *In vitro*, *NOTCH1* downregulation inhibited proliferation of glioblastoma cells (Fig. 7D); *in vivo*, tumor bearing mice showed an improved survival when *NOTCH1* was downregulated (Fig. 7E). High-field MRI confirmed the brain tumor growth attenuation after *NOTCH1* knockdown (Fig. 7F,G). In contrast, after irradiation, the small and growth-deficient brain tumors were highly therapy resistant, with no regression being detectable compared to sham treatment (Fig. 7F,G). In summary, *NOTCH1* proficiency plays an important role for the colonization of the PVN and tumor growth, whereas its deficiency results in impaired growth but also induces TM- and network formation that makes the tumor more radioresistant (Fig. 8).

Discussion

The dynamics, fate, and relevance of individual glioma cells in the perivascular niche was revealed for the first time in this study over weeks and months. In line with previous work investigating tumor cell dynamics in different tumor areas [32], tumor cell invasion was not restricted to the invasive front but also prevalent in the dense tumor core. Here, we show that these dynamics are characteristic for parenchymal cells, whereas a majority of perivascular cells shows residency, even at the invasive front. The go-or-grow hypothesis suggests that glioma cells either migrate or proliferate [33]. Our data suggests that the invading parenchymal cells constitute the proliferating subpopulation, which is in line with recent single cell analyses [34], arguing for a go-*and*-grow (and not go-*or*-grow) mechanism that should be further investigated in future studies. A minority of the resident perivascular cells was closely associated with remodeled blood vessels forming capillary loops or glomeroloid bodies [35], further suggesting reciprocity in the perivascular niche [8, 10]. Previous studies demonstrated that glomeroloid bodies are populated by stem-like tumor cells in human tumor specimen [36] and this microvascular pattern is associated with a worse outcome in patients [37, 38].

During neurogenesis, the PVN provides a specific microenvironment for neural stem cells [39]. A similar PVN for cancer stem-like cells has been proposed for primary brain tumors [6, 7, 10, 12] and these stem-like cells have been associated with therapy resistance and tumor recurrence [2, 6, 7, 40]. Recently, a metabolic zonation and consequent cellular heterogeneity dependent on the distance from blood vessels have been demonstrated in gliomas and perivascular cells exhibited a more aggressive phenotype and pronounced therapy resistance [41]. Our data confirms that tumor cells in the perivascular region are highly resistant against cytotoxic therapies, largely independent of the integration into multicellular networks. If this resistance is due to the slower proliferation rate, metabolic differences and/or specific microenvironmental cues, such as *NOTCH1* signaling discussed below, remains to be elucidated. Here,

despite its residency, perivascular glioma cells demonstrated reactiveness to nearby damage by inducing an early gliotic reaction, thereby sharing traits with neural stem cells [42] and reactive astrocytes, which also possess stem cell features [43].

Endothelial cells are known to activate *NOTCH1* signaling in adjacent glioma cells, including glioma stem-like cells [4, 7, 8, 26]. *NOTCH1* inhibitors have been tried in various preclinical studies, partially demonstrating effects on stem-like cells, although conflicting data exists and evidence for efficacy in clinical trials is still lacking [44, 45]. Making use of the shRNA mediated knockdown of *NOTCH1* we provide one possible explanation for those conflicting results: Although downregulation of *NOTCH1* led to a depletion of the perivascular cell population, reduced tumor growth and reduced therapy resistance of cells in the PVN, it also induced TM- and network formation, thereby rendering the growth-deficient tumors virtually unsusceptible for the cytotoxic effects of radiotherapy. *NOTCH1* proficiency is hence a key mechanism for the resilience of cells in the PVN, firstly by allowing population of that niche and secondly by being prerequisite for the protective properties of this specific microenvironment. In line with our results outlined here, many publications demonstrate a growth-inhibitory effect of *NOTCH1* downregulation [44, 46, 47, 48, 49, 50]. The differences regarding response to cytotoxic therapies [46, 47, 48, 49, 50] might be explained by the different models used and their TM-proficient phenotype. Our data suggests that *NOTCH1* is an important mediator of the resistance of perivascular tumor cells and the resistance promoting effects of *NOTCH1* downregulation can be attributed to the induction of TMs. The latter might not be reflected in all models: especially cultivation under serum-containing conditions, which were used for many studies on *NOTCH1* in glioblastoma [49], leads to TM-deficient tumors [17].

The formation of TMs shares many features with axon and neurite outgrowth, which is underlined by the phenotype observed after *NOTCH1* knockdown. During neurodevelopment, *NOTCH1* activation inhibits neurite sprouting [28, 51], whereas *NOTCH1* inhibition has been shown to promote neurite extension [52]. Interestingly, *NOTCH1* has recently been identified as a positive regulator of tweety homolog 1 (*TTYH1*) expression [53], which is an important driver of the formation of TMs involved in tumor cell invasion [17]. *TTYH1* downregulation leads to growth-deficient but highly interconnected tumors [17] thereby resembling the phenotype after *NOTCH1* downregulation.

Our data suggests that *NOTCH1* inhibition might be used to slow down tumor growth but should be avoided in combination with cytotoxic therapies due to the induction of tumor cell networks. In TM-deficient oligodendrogliomas, we found an upregulation of the NOTCH1 pathway, both in the BT088 cell line and human samples. We were not able to induce TM extension by *NOTCH1* knockdown though, likely due to the general TM growth deficiency of these tumors.

Thus, our data implies that at least two, partially additive and complementary, niches of cellular resilience exist in glioblastoma: a PVN and a TM connectivity niche, that inversely depend on *NOTCH1* expression. Phenotypic adaptation [54] or switches between both niches must be considered for targeted therapies.

In conclusion, the perivascular compartment accommodates the majority of long-term resident glioma cells and is associated with resistance against cytotoxic therapies. Downregulation of the *NOTCH1* pathway depletes this cell pool and diminishes the protective properties of the perivascular niche, but concomitantly induces TM- and network formation with subsequent therapy resistance. All in all, this describes two niches of progression and resistance in gliomas - the TM connectivity niche and the PVN – and speaks for a complex and partially complementary role of these two. To effectively treat incurable astrocytomas and glioblastomas, novel concepts to target both niches seem of high importance, ideally avoiding cross-compensatory tumor cell reactions.

Methods

Cell lines: The patient-derived glioblastoma cell lines S24, T269, T325 and P3xx and BT088 oligodendroglioma cells were kept under stem-like neurosphere conditions (37 °C, 5.0% CO2): DMEM F-12 medium (31330-038, Invitrogen), B27 supplement (12587-010, Invitrogen), 5 µg ml − 1 insulin (I9278, Sigma-Aldrich), 5 µg ml − 1 heparin (H4784, Sigma-Aldrich), 20 ng ml − 1 epidermal growth factor (rhEGF; 236-EG, R&D Systems), and 20 ng ml − 1 basic fibroblast growth factor (bFGF; PHG0021, Thermo Fisher Scientific). S24 (human, female), T269 (human, male), T325 (human, male) and P3xx (human) were authentificated (Multiplexion GmbH, Germany). S24, T269 and T325 were further authenticated as glioblastoma by Illumina 850 k methylation array. BT088 cells were obtained from ATCC (ATCC CRL-3417, RRID:CVCL_N708) (human, male).

Lentiviral Transductions: For transduction, cells were incubated with lentiviral particles and 10 µg ml − 1 polybrene (TR-1003-G, Merck Millipore) for 24 h. Cell lines were stably transduced with the LeGO-T2 vector (cytoplasmatic tdTomato, Addgene 27342, RRID:Addgene_27342), pLKO.1-LV-GFP (H2B-GFP, Addgene #25999, RRID:Addgene_25999), pLenti6.2 hygro/V5-Lifeact-YFP, plKO.1-puro-CMV-TurboGFP_shnon-target (cytoplasmatic GFP, SHC016, Sigma-Aldrich), plKO.1-puro-CMV-TurboGFP_shCX43 (*CX43* knockdown, sequence: GCCCAAACTGATGGTGTCAA, Sigma-Aldrich), and plKO.1-puro-CMV-TurboGFP_shNOTCH1 (*NOTCH1* knockdown, sequence: CCGGGACATCACGGATCATAT, Sigma-Aldrich). *NOTCH1* and *CX43* knockdown were confirmed by western blot analysis (45% (S24 GBMSCs); 92% (BT088) (*NOTCH1*) / 80% (S24 GBMSCs) (*CX43*) reduction in protein expression). Anti-Notch1 (#4380, Cell Signaling Technology, RRID:AB_10691684) and anti-GAPDH antibody (LAH1064, Linaris) were used for western blot analyses.

Animal Procedures: 8-to-10-week-old male NMRI nude mice (Charles River) were used for studying the intracranial tumor growth and dynamics. All animal procedures were performed in accordance with the institutional laboratory animal research guidelines after approval of the Regierungspräsidium Karlsruhe, Germany. A chronic cranial window and a titan ring that allows pain-free fixation of the animals during two photon microscopy were implanted as described before [15, 17]. Two weeks after window implantation 30,000 patient-derived and fluorescently labeled glioblastoma stem-like cells suspended in PBS were intracranially implanted in a depth of 500 µm. For survival and MRI studies, 50,000 cells (S24 shControl and shNotch1) were implanted without preparation of a chronic cranial window. T2-weighted rapid

acquisition with refocused echoes sequence MRI images were acquired on a 9.4 T horizontal bore MR scanner (BioSpec 94/20 USR, Bruker BioSpin) with a four-channel phased-array surface coil (parameters: TE = 33 ms, TR = 2500 ms, flip angle = 90°, acquisition matrix: 200 × 150, number of averages = 2, slice thickness = 700 µm duration = 2 min 53 s). For radiotherapy experiments, whole brain irradiation with fractions of 7 Gy at a dose rate of 3 Gy min − 1 were performed on 3 consecutive days at D60 (± 10 days) using a 6 MV linear accelerator (Artiste, Siemens) with a 6 mm collimator adjusted to the window size. As control no radiation was applied (sham radiation). For chemotherapy experiments, mice were treated with 100 mg/kg body weight temozolomide for 3 consecutive days on D85 ± 3 after tumor implantation by oral gavage. For two photon microscopy and MRI imaging mice were anesthetized with isoflurane. Mice were scored clinically and rapidly killed if they showed neurological symptoms or a weight loss of > 20%.

In Vivo Multiphoton Laser Scanning Microscopy: Intravital 2-photon microscopy (2-PM) was performed with a Zeiss 7MP microscope (Zeiss) equipped with a Coherent Chameleon UltraII laser (Coherent) on anesthetized mice (4% isoflurane for initiation, 0.5-2% for maintenance of anesthesia). A custom-made aperture allowed painless fixation of the head for imaging. Body temperature was permanently controlled by a rectal thermometer and was kept constant by a heating pad. Angiograms allowed identification of the same tumor regions over time. For angiograms, fluorescent dextranes (10 mg ml-1, TRITC-dextrane (500 kDa; 52194, Sigma Aldrich) or FITC-dextrane (2,000 kDa, FD2000S, Sigma Aldrich)) were applied by tail vein injection. The following wavelengths were used for excitation of different fluorophores: 750 nm (FITC-dextrane, tdTomato), 850 nm (GFP, TRITC-dextrane) and 950 nm (tdTomato, YFP). Appropriate filter sets (band pass 500–550 nm/band pass 575–610 nm) were used. For ablation of single glioma cells, the laser beam was focused on the GFP-labeled nucleus (H2B-GFP) and continuous scanning was performed until disintegration of the cell. For damage of a larger tumor area, repetitive scanning (950 nm wavelength) for approximately 8 minutes with high laser power was performed. For the evaluation of therapeutic responses, the same tumor regions were imaged repetitively over one to three weeks. For invasion speed measurements and identification of invading tumor cells, single glioma cells were followed with repetitive imaging over 24 hours. Short-term residency of individual glioma cells was determined by repetitive imaging over 4 (S24) and 5 days (P3xx), long-term residency by repetitive imaging between D41 and D62.

SR101 staining and separation of connected and unconnected tumor cells

For separation of connected and unconnected tumor cells, mice bearing S24 and T269 GFP tumors were injected with sterilized saline solution dissolving SR101 (S359, Invitrogen) i.p. at a dose of 0.12 mg per gram body weight, which is taken up by tumor cells within 5–8 hours. Mice were then perfused with PBS and the brains were harvested. Whole brain single cell suspensions were prepared with brain tumor dissociation kit (130-095-942, Miltenyi Biotec) and gentleMACSTM Dissociator (Miltenyi Biotec). After dissociation the suspension was resuspended in FACS buffer (PBS + 1% FCS, 10500064, ThermoFisher). FACS was performed on a FACSAria cell sorter (BD Biosystems). Cells were stained with Calcein Violet 450 AM (65-0854-39, Invitrogen) and TO-PRO®-3 Iodide (T3605, Invitrogen) for 10 min on ice before sorting for the viable cell population (Calcein Violet 450high and TO-PRO-3neg). Within the viable cell

population SR101high, GFP+ (connected tumor cells) and SR101low, GFP+ (unconnected tumor cells) were separated. The YG586/15 channel was used to visualize SR101 signal.

Bulk RNA sequencing of connected and unconnected tumor cells

After cell sorting, cell populations were lysed (lysis buffer, RNeasy Micro Kit, 74004, Qiagen). mRNA was isolated and purified in accordance with the manufacturer's instruction. The conversion of RNA to dsDNA was done with the SMARTer Ultra Low Input RNA for Illumina Sequencing (Clontech), the libraries were then prepared using NEBNext® ChIP-Seq Library Prep Master Mix Set for Illumina (E6240, New England Biolabs) and sequenced on HiSeq2000 v4 (Illumina) in 50 bp single-end mode by our core facility. The quality of bases was evaluated using the FASTX Toolkit. Homertools 4.7 were applied for PolyA-tail trimming [55]; reads with a length of < 17 were removed. The filtered reads were mapped with STAR 2.3 [56] against the human reference genome (GRCh38) and PicardTools 1.78 with CollectRNASeqMetrics were used for quality checking. Count data were generated by htseq-count using the gencode.v26.annotation.gtf file for annotation [57]. DESeq2 1.4.1 was run with default parameters for the group-wise comparison [58]. The expression levels were transformed to logarithmic space using log2. The RNA sEq. data of connected and unconnected S24 and T269 glioblastoma cells will be deposited in the Gene Expression Omnibus under accession no.(tbd) and is available upon request.

Analysis of differential mRNA expression of human gliomas

RNA sequencing data of molecular (1p/19q-codeleted, IDH mutant) oligodendroglioma (n = 56) and molecular (1p/19q non-codeleted, IDH wildtype) glioblastoma (n = 70) was downloaded from TCGA and analyzed as described previously [15]. The full list of differentially expressed genes can be found in Osswald et al., 2015 [15].

Immunofluorescence and confocal microscopy: For immunofluorescence of mouse tissue, tumor bearing mice were cardially perfused with PBS, followed by 4.5% phosphate-buffered formaldehyde solution (Roti-Histofix 4.5%, 2213, Carl Roth). Brain tissue was incubated in 30% sucrose solution overnight for cryoprotection and snap frozen afterwards. Heat-induced epitope retrieval with 0.01 M citrate buffer, pH 6.0, was performed. The following primary antibodies were used: anti-nestin (1:400, ab6320, Abcam, RRID:AB_308832), anti-CD31 (1:100, AF3628, R&D Systems, RRID:AB_2161028), anti-aquaporin 4 (1:200, ab9512, Abcam, RRID:AB_307299), anti-activated Notch1 (1:50, ab8925, Abcam, RRID:AB_306863) and anti-ki67 (1:500, ab15580, Abcam, RRID:AB_443209). Donkey anti-mouse IgG Alexa Fluor 488 (A-21202, Thermo Fisher Scientific, RRID:AB_141607), goat anti-mouse IgG Alexa Fluor 488 conjugate (A-11029, Thermo Fisher Scientific, RRID:AB_138404), donkey anti-goat IgG Alexa Fluor 633 (A-21082, Thermo Fisher Scientific, RRID:AB_141493) and donkey anti-rabbit IgG Alexa Fluor 546 (A-10040, Thermo Fisher Scientific, RRID:AB_2534016) secondary antibodies were used. Images were acquired using a Leica TCS SP5 confocal microscope.

Immunohistochemical and immunofluorescence staining of human tumor specimen: Tissue sections of resected primary gliomas were obtained from the Department of Neuropathology in Heidelberg in accordance with local ethical approval. Sections were incubated with the anti-IDH1 R132H antibody (H09, Dianova, RRID:AB_2335716). 3 µm thin formalin-fixed paraffin-embedded and 100 µm thick sections formalin-fixed tissue sections were used for immunohistochemistry and immunofluorescence respectively.

Alamar blue proliferation assay: 1000 GBMSCs were seeded in 96-well plates and AlamarBlue Reagent (DAL1025, Thermo Fisher Scientific) was added on days 0, 1, 3, and 5. Fluorescence intensity (excitation: 560 nm; emission: 590 nm) was measured using a SpectraMax M5e microplate reader (Molecular Devices) after 3 h.

Image Processing: For image analysis and figures, images were processed using ZEN software (Zeiss, RRID:SCR_018163) and Imaris (Bitlane, RRID:SCR_007370). Image calculation and filtering was performed to reduce background noise. For figures, 3D stacks are transformed into orthogonal 2D maximum intensity projections (MIP).

Quantifications: All quantifications were performed manually in ImageJ (NIH, RRID:SCR_003070) and Imaris (Bitlane, RRID:SCR_007370) in high resolution (1024*1024 pixels) 3D z-stacks. Cells were regarded perivascular if the whole cell body was directly associated with a blood vessel. TM length of individual cells was measured by tracking TMs in z-stacks (3D images). For the mitotic index, mitotic events were analyzed in H2B-GFP expressing cells. The mitotic events were normalized to the distribution of cells in the parenchymal and perivascular compartment in the respective region, thereby assuming equal fractions in both compartments. The early reaction after single ablation was defined as the directed extension of TMs towards the damaged area within 100 minutes. For the quantification of the tumor/brain area ratio on MRI images, the tumor and the whole-brain area were measured manually in the image with the largest tumor expansion.

Statistics: Statistical analyses were performed using SigmaPlot (Systat Software, RRID:SCR_003210). Normal distribution of datasets was assessed with a Shapiro–Wilk test. Statistical significance of normally distributed data was assessed by a two-sided Student's t test. Non-normally distributed data were assessed with a Mann–Whitney rank-sum test. For datasets with > 2 groups ANOVA or ANOVA on ranks with the appropriate post hoc tests (Tukey's or Student–Newman–Keuls tests) were performed. Statistical details including can be found in the respective figure legends.

Declarations

Competing interests:

E.J., M.O., W.W. and F.W. report the patent (WO2017020982A1) “Agents for use in the treatment of glioma“. F.W. is co-founder of DC Europa Ltd (a company trading under the name Divide & Conquer) that

is developing new medicines for the treatment of glioma. Divide & Conquer also provides research funding to FW's lab under a research collaboration agreement.

Author contributions:

E.J., M.O., W.W. and F.W. designed the study, interpreted the data and wrote the manuscript. E.J. and M.O. analyzed data. E.J., M.O., M.R. and S.W. performed two photon microscopy imaging. R.X. performed FACS and RNA-sEq. analyses. E.J. performed immunofluorescence stainings. F.K. and S.H. performed MRI imaging and interpreted the data. F.S. and A.v.D. performed and interpreted immunohistochemical stainings.

Acknowledgments:

We thank Hrvoje Miletic for providing the P3 cell line. We thank Miriam Gömmel and Susann Wendler for technical assistance. This study was funded by grants from the German Research Foundation (DFG, SFB 1389) to W.W., F.W., E.J. and M.R., and to F.K. (DFG, KU 3555/1–1). F.S. is fellow of the Else Kröner Excellence Program of the Else Kröner-Fresenius Stiftung (EKFS).

References

1. Weller M, *et al.* Glioma. *Nat Rev Dis Primers* **1**, 15017 (2015).
2. Galli R, *et al.* Isolation and characterization of tumorigenic, stem-like neural precursors from human glioblastoma. *Cancer Res* **64**, 7011–7021 (2004).
3. Ignatova TN, Kukekov VG, Laywell ED, Suslov ON, Vrionis FD, Steindler DA. Human cortical glial tumors contain neural stem-like cells expressing astroglial and neuronal markers in vitro. *Glia* **39**, 193–206 (2002).
4. Lathia JD, Mack SC, Mulkearns-Hubert EE, Valentim CL, Rich JN. Cancer stem cells in glioblastoma. *Genes Dev* **29**, 1203–1217 (2015).
5. Lathia JD, *et al.* Direct in vivo evidence for tumor propagation by glioblastoma cancer stem cells. *PLoS One* **6**, e24807 (2011).
6. Calabrese C, *et al.* A perivascular niche for brain tumor stem cells. *Cancer Cell* **11**, 69–82 (2007).
7. Charles N, *et al.* Perivascular nitric oxide activates notch signaling and promotes stem-like character in PDGF-induced glioma cells. *Cell Stem Cell* **6**, 141–152 (2010).
8. Lathia JD, Heddleston JM, Venere M, Rich JN. Deadly teamwork: neural cancer stem cells and the tumor microenvironment. *Cell Stem Cell* **8**, 482–485 (2011).
9. Hjelmeland AB, Lathia JD, Sathornsumetee S, Rich JN. Twisted tango: brain tumor neurovascular interactions. *Nat Neurosci* **14**, 1375–1381 (2011).

10. Gilbertson RJ, Rich JN. Making a tumour's bed: glioblastoma stem cells and the vascular niche. *Nat Rev Cancer* **7**, 733–736 (2007).
11. Alvarez-Buylla A, Kohwi M, Nguyen TM, Merkle FT. The heterogeneity of adult neural stem cells and the emerging complexity of their niche. *Cold Spring Harb Symp Quant Biol* **73**, 357–365 (2008).
12. Charles N, Holland EC. The perivascular niche microenvironment in brain tumor progression. *Cell Cycle* **9**, 3012–3021 (2010).
13. Filbin M, Monje M. Developmental origins and emerging therapeutic opportunities for childhood cancer. *Nat Med* **25**, 367–376 (2019).
14. Lee JH, *et al.* Human glioblastoma arises from subventricular zone cells with low-level driver mutations. *Nature* **560**, 243–247 (2018).
15. Osswald M, *et al.* Brain tumour cells interconnect to a functional and resistant network. *Nature* **528**, 93–98 (2015).
16. Jung E, Alfonso J, Osswald M, Monyer H, Wick W, Winkler F. Emerging intersections between neuroscience and glioma biology. *Nat Neurosci* **22**, 1951–1960 (2019).
17. Jung E, *et al.* Tweety-Homolog 1 Drives Brain Colonization of Gliomas. *J Neurosci* **37**, 6837–6850 (2017).
18. Weil S, *et al.* Tumor microtubes convey resistance to surgical lesions and chemotherapy in gliomas. *Neuro Oncol*, (2017).
19. Sahm F, *et al.* Addressing diffuse glioma as a systemic brain disease with single-cell analysis. *Arch Neurol* **69**, 523–526 (2012).
20. Capper D, *et al.* Characterization of R132H mutation-specific IDH1 antibody binding in brain tumors. *Brain Pathol* **20**, 245–254 (2010).
21. Venkataramani V, *et al.* Glutamatergic synaptic input to glioma cells drives brain tumour progression. *Nature* **573**, 532–538 (2019).
22. Venkatesh HS, *et al.* Electrical and synaptic integration of glioma into neural circuits. *Nature* **573**, 539–545 (2019).
23. Koga T, *et al.* Longitudinal assessment of tumor development using cancer avatars derived from genetically engineered pluripotent stem cells. *Nat Commun* **11**, 550 (2020).
24. Chen J, *et al.* A restricted cell population propagates glioblastoma growth after chemotherapy. *Nature* **488**, 522–526 (2012).
25. Alieva M, *et al.* Preventing inflammation inhibits biopsy-mediated changes in tumor cell behavior. *Sci Rep* **7**, 7529 (2017).
26. Zhu TS, *et al.* Endothelial cells create a stem cell niche in glioblastoma by providing NOTCH ligands that nurture self-renewal of cancer stem-like cells. *Cancer Res* **71**, 6061–6072 (2011).
27. Bayin NS, *et al.* Notch signaling regulates metabolic heterogeneity in glioblastoma stem cells. *Oncotarget* **8**, 64932–64953 (2017).

28. Sestan N, Artavanis-Tsakonas S, Rakic P. Contact-dependent inhibition of cortical neurite growth mediated by notch signaling. *Science* **286**, 741–746 (1999).
29. Osswald M, Solecki G, Wick W, Winkler F. A malignant cellular network in gliomas: potential clinical implications. *Neuro Oncol* **18**, 479–485 (2016).
30. van den Bent MJ, *et al.* Adjuvant procarbazine, lomustine, and vincristine chemotherapy in newly diagnosed anaplastic oligodendroglioma: long-term follow-up of EORTC brain tumor group study 26951. *J Clin Oncol* **31**, 344–350 (2013).
31. Cairncross JG, *et al.* Benefit from procarbazine, lomustine, and vincristine in oligodendroglial tumors is associated with mutation of IDH. *J Clin Oncol* **32**, 783–790 (2014).
32. Alieva M, Leidgens V, Riemenschneider MJ, Klein CA, Hau P, van Rheenen J. Intravital imaging of glioma border morphology reveals distinctive cellular dynamics and contribution to tumor cell invasion. *Sci Rep* **9**, 2054 (2019).
33. Giese A, Bjerkvig R, Berens ME, Westphal M. Cost of migration: invasion of malignant gliomas and implications for treatment. *J Clin Oncol* **21**, 1624–1636 (2003).
34. Wang L, *et al.* The Phenotypes of Proliferating Glioblastoma Cells Reside on a Single Axis of Variation. *Cancer Discov* **9**, 1708–1719 (2019).
35. Rojiani AM, Dorovini-Zis K. Glomeruloid vascular structures in glioblastoma multiforme: an immunohistochemical and ultrastructural study. *J Neurosurg* **85**, 1078–1084 (1996).
36. Chen J, *et al.* The pathological structure of the perivascular niche in different microvascular patterns of glioblastoma. *PLoS One* **12**, e0182183 (2017).
37. Chen L, *et al.* Classification of microvascular patterns via cluster analysis reveals their prognostic significance in glioblastoma. *Hum Pathol* **46**, 120–128 (2015).
38. Birner P, *et al.* Vascular patterns in glioblastoma influence clinical outcome and associate with variable expression of angiogenic proteins: evidence for distinct angiogenic subtypes. *Brain Pathol* **13**, 133–143 (2003).
39. Bjornsson CS, Apostolopoulou M, Tian Y, Temple S. It takes a village: constructing the neurogenic niche. *Dev Cell* **32**, 435–446 (2015).
40. Singh SK, *et al.* Identification of a cancer stem cell in human brain tumors. *Cancer Res* **63**, 5821–5828 (2003).
41. Kumar S, *et al.* Intra-Tumoral Metabolic Zonation and Resultant Phenotypic Diversification Are Dictated by Blood Vessel Proximity. *Cell Metab* **30**, 201–211 e206 (2019).
42. Arvidsson A, Collin T, Kirik D, Kokaia Z, Lindvall O. Neuronal replacement from endogenous precursors in the adult brain after stroke. *Nat Med* **8**, 963–970 (2002).
43. Robel S, Berninger B, Gotz M. The stem cell potential of glia: lessons from reactive gliosis. *Nat Rev Neurosci* **12**, 88–104 (2011).
44. Bazzoni R, Bentivegna A. Role of Notch Signaling Pathway in Glioblastoma Pathogenesis. *Cancers (Basel)* **11**, (2019).

45. Xu R, *et al.* Molecular and Clinical Effects of Notch Inhibition in Glioma Patients: A Phase 0/I Trial. *Clin Cancer Res* **22**, 4786–4796 (2016).
46. Han N, *et al.* Notch1 ablation radiosensitizes glioblastoma cells. *Oncotarget* **8**, 88059–88068 (2017).
47. Wang J, *et al.* Notch promotes radioresistance of glioma stem cells. *Stem Cells* **28**, 17–28 (2010).
48. Hai L, *et al.* Notch1 is a prognostic factor that is distinctly activated in the classical and proneural subtype of glioblastoma and that promotes glioma cell survival via the NF-kappaB(p65) pathway. *Cell Death Dis* **9**, 158 (2018).
49. Gersey Z, *et al.* Therapeutic Targeting of the Notch Pathway in Glioblastoma Multiforme. *World Neurosurg* **131**, 252–263 e252 (2019).
50. Yahyanejad S, *et al.* NOTCH blockade combined with radiation therapy and temozolomide prolongs survival of orthotopic glioblastoma. *Oncotarget* **7**, 41251–41264 (2016).
51. Berezovska O, *et al.* Notch1 inhibits neurite outgrowth in postmitotic primary neurons. *Neuroscience* **93**, 433–439 (1999).
52. Liu M, Inoue K, Leng T, Zhou A, Guo S, Xiong ZG. ASIC1 promotes differentiation of neuroblastoma by negatively regulating Notch signaling pathway. *Oncotarget* **8**, 8283–8293 (2017).
53. Wu HN, *et al.* Deficiency of Ttyh1 downstream to Notch signaling results in precocious differentiation of neural stem cells. *Biochem Biophys Res Commun* **514**, 842–847 (2019).
54. Celiku O, Gilbert MR, Lavi O. Computational modeling demonstrates that glioblastoma cells can survive spatial environmental challenges through exploratory adaptation. *Nat Commun* **10**, 5704 (2019).
55. Heinz S, *et al.* Simple combinations of lineage-determining transcription factors prime cis-regulatory elements required for macrophage and B cell identities. *Mol Cell* **38**, 576–589 (2010).
56. Dobin A, *et al.* STAR: ultrafast universal RNA-seq aligner. *Bioinformatics* **29**, 15–21 (2013).
57. Anders S, Pyl PT, Huber W. HTSeq–a Python framework to work with high-throughput sequencing data. *Bioinformatics* **31**, 166–169 (2015).
58. Love MI, Huber W, Anders S. Moderated estimation of fold change and dispersion for RNA-seq data with DESeq2. *Genome Biol* **15**, 550 (2014).

Figures

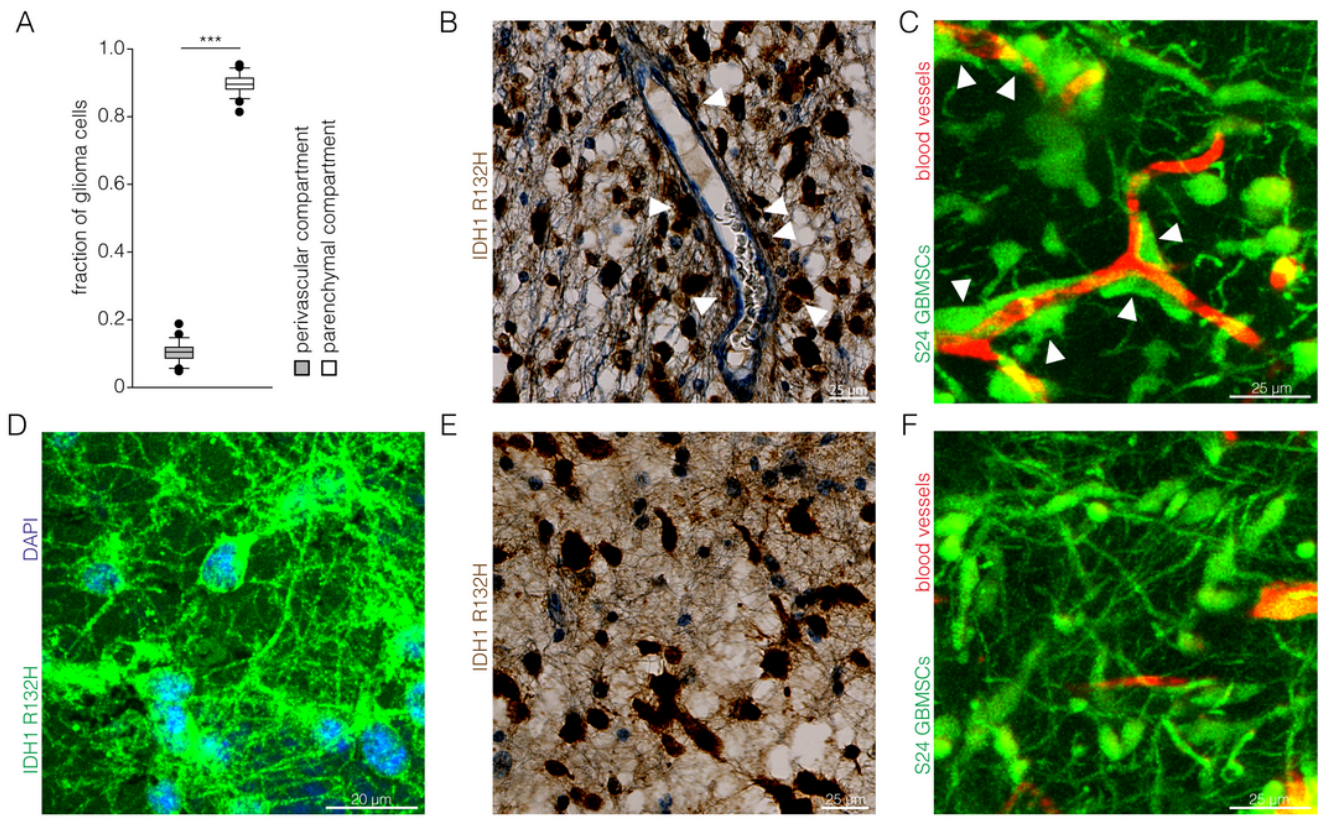

Figure 1

Figure 1

The perivascular and network niches in human and experimental gliomas (A) Distribution of IDH1 R132H positive glioma cells in the perivascular and parenchymal compartment in patient glioma specimen (n=14 patients; t-test). (B) Exemplary immunohistochemical staining of IDH1 R132H in a human astrocytoma specimen demonstrates the close association of tumor cells with a blood vessel (arrowheads). (C) Intravital 2-PM image of perivascular S24 glioblastoma cells (arrowheads) in a mouse xenograft. (D) Exemplary confocal IDH1 R132H mutation-specific immunofluorescence image of a human astrocytoma specimen demonstrates dense interconnection of glioma cells. (E) Mutation-specific immunohistochemical staining of IDH1 R132H in a human astrocytoma specimen shows dense interconnection of glioma cells in the parenchymal compartment. (F) Exemplary 2-PM image of highly interconnected S24 GBMSCs growing in the mouse brain.

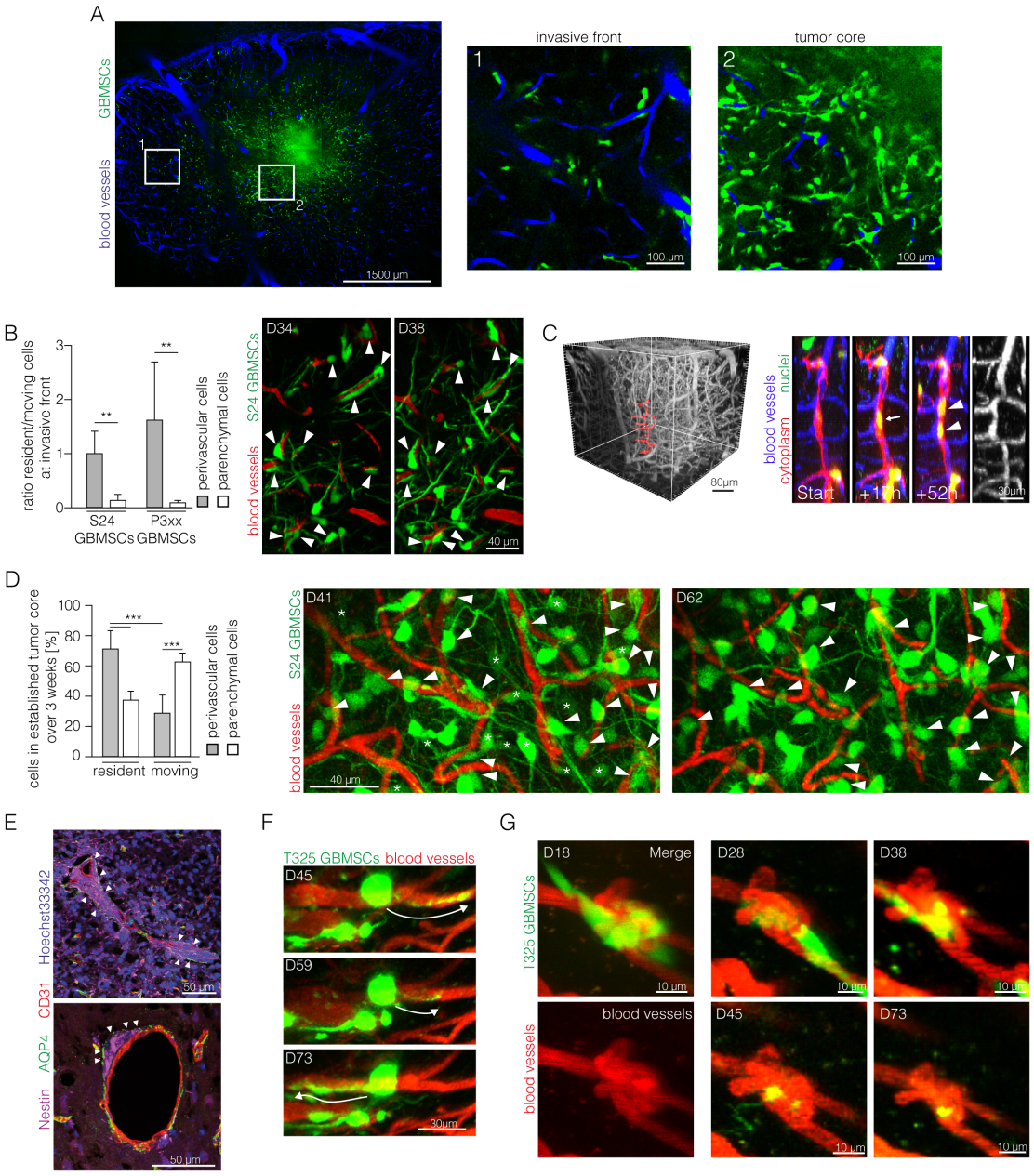

Figure 2

Figure 2

Long-term glioma cell behaviour in the perivascular niche (A) Overview intravital 2-PM image of the tumor bearing hemisphere (S24 GBMSCs, D23). Right: Magnifications show the invasive front (1) and the tumor core (2). (B) Left: Ratio of resident and moving S24 and P3xx GBMSCs at the invasive front over 4 (S24) and 5 (P3xx) days (n=3 mice per cell line, 41-86 cells in 4 regions (S24) / 23-57 cells in 5 regions (P3xx), t-test (S24) and Mann Whitney test (P3xx)). Right: Exemplary intravital 2-PM images of the same region at

the invasive front imaged over 4 days demonstrating several resident perivascular cells (arrowheads) (S24 GBMSCs, D34-38). (C) Left: 3D in vivo 2-PM image of the vasculature. The vessels shown on the right side are marked in red. Right: Timeseries of resident and dividing S24 GBMSC (arrow) in the perivascular niche over 52 hours. Daughter nuclei (arrow heads). The angiogram is shown on the right. Blood vessels (blue), nuclei (green), cytoplasm (red). (D) Left: Analysis of residency and migration in the established tumor core over 21 days (D41-62) (S24 GBMSCs, in vivo 2-PM, n=3 mice, 46-81 cells in 5 regions, ANOVA). Right: Exemplary intravital 2-PM images of the same region at day 41 and 62. Resident perivascular S24 GBMSCs are marked with arrowheads, moving parenchymal cells are marked by asterisks. (E) Immunofluorescence staining of nestin (purple), Aquaporin 4 (AQP4) (green), CD31 (red) and Hoechst33342 (blue) demonstrates the localization of perivascular cell clusters below the astrocyte endfeet (S24 GBMSCs). (F) Exemplary in vivo 2-PM images of T325 GBMSCs over 28 days showing a resident tumor cell extending and retracting TMs (arrows). (G) Repetitive 2-PM imaging of T325 GBMSCs (green) demonstrating a resident cell associated with a remodeled blood vessel (red). Data (B,D) are represented as mean ± SD.

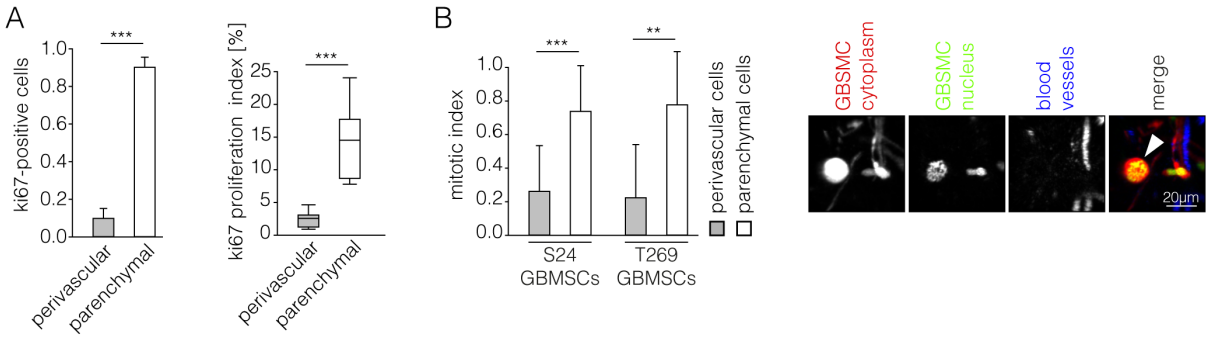

Figure 3

Figure 3

Perivascular cells are slow-cycling (A) Left: Distribution of ki67-positive cells in the perivascular and parenchymal compartment in S24 tumors (n=3 mice, 16 regions, t-test). Right: ki67 proliferation index (ki67 positive cells/all cells in the respective compartment) of S24 tumor cells in the perivascular and the parenchymal compartment (n=3 mice, 7 regions, t-test). (B) Mitotic index (number of mitotic events normalized to the distribution of cells in the perivascular and parenchymal compartment) of S24 and T269 GBMSCs (n=8 mice (S24), n= 4 mice (T269), Mann Whitney tests). Data are represented as median, IQR and P10/P90. Right: Exemplary in vivo 2-PM of mitosis of a parenchymal S24 GBMSC (arrow head). Cytoplasm (red), nucleus (green), blood vessels (blue). Data (A,C) are represented as mean ± SD.

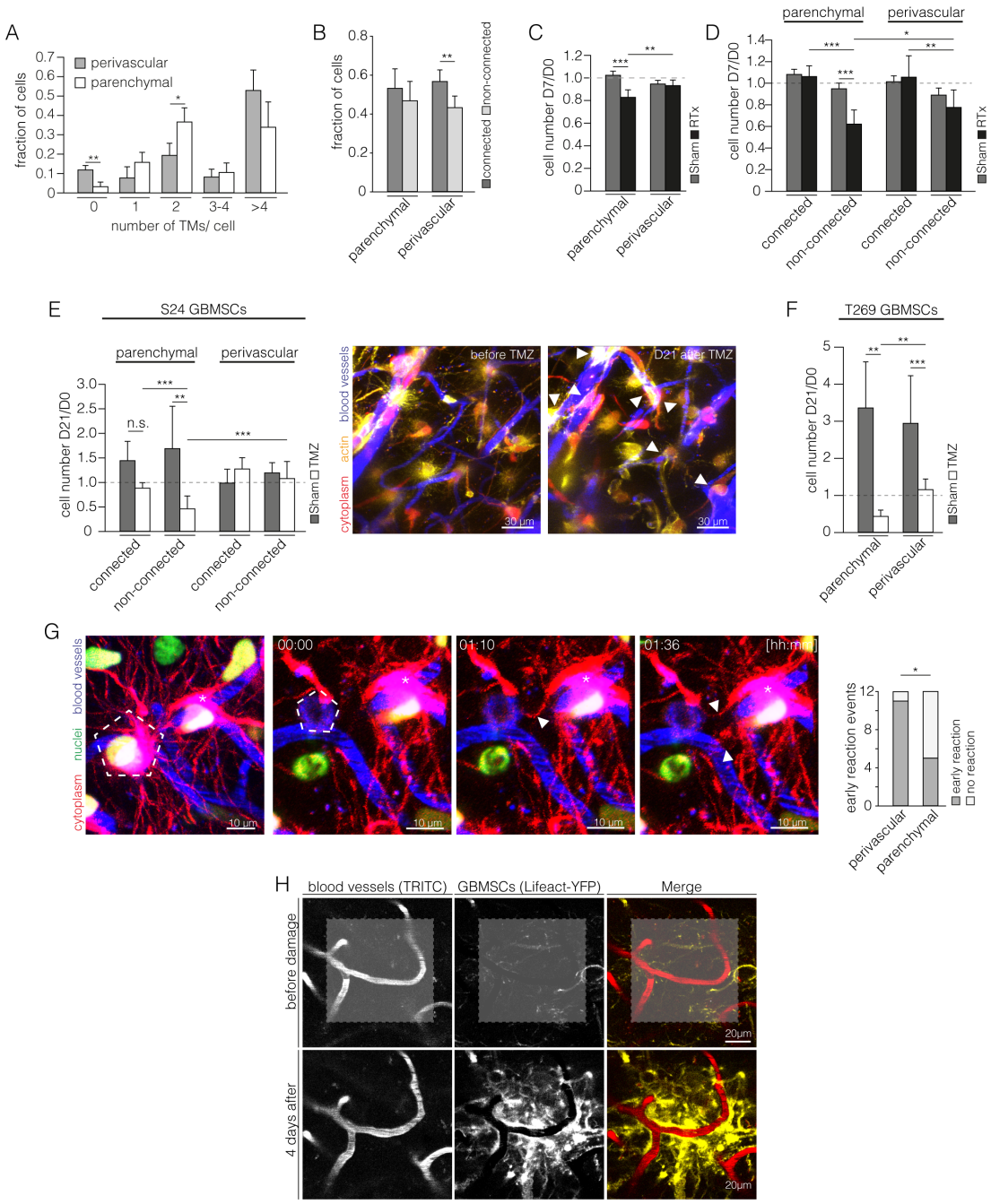

Figure 4

Figure 4

Both perivascular and network glioma cells are particularly resilient (A) Analysis of fractions of cells with different number of TMs (S24 GBMSCs, D41, n=3 mice, 52-104 cells, t-tests). (B) Analysis of the connectivity of cells in the perivascular and parenchymal compartment (S24 GBMSCs, D65 ± 4, n=6 mice, 10 regions, 148-259 cells, ANOVA). (C), (D) Ratio of tumor cell counts in the same regions 7 days after and before sham treatment or irradiation (RTx) (S24 GBMSCs, n=3 mice per group, ANOVAs). (E) Left:

Ratio of cell counts of S24 GBMSCs in the same regions 21 days after and before temozolomide or sham treatment (n=3 mice per group, ANOVA on ranks). Right: Exemplary 2-PM before and 21 days after temozolomide treatment in S24 GBMSCs. Triangles: surviving perivascular GBMSCs. (F) Ratio of cell counts of T269 GBMSCs in the same regions 21 days after and before temozolomide or sham treatment (n=3 mice per group, ANOVA on ranks). (G) Left: Early reaction (white triangles) of a perivascular cell (asterisk) after laser ablation of a nearby S24 GBMSC (pentagon). Cytoplasm (red), blood vessels (blue), nuclei (green). Right: Analysis of the early reaction to laser ablation of nearby cells (S24 GBMSCs, n=12 events, Fisher exact test). (H) After laser-induced stress (marked with grey area in the upper row) a strong perivascular reaction can be observed (S24 GBMSCs). Data (A-F) are represented as mean ± SD.

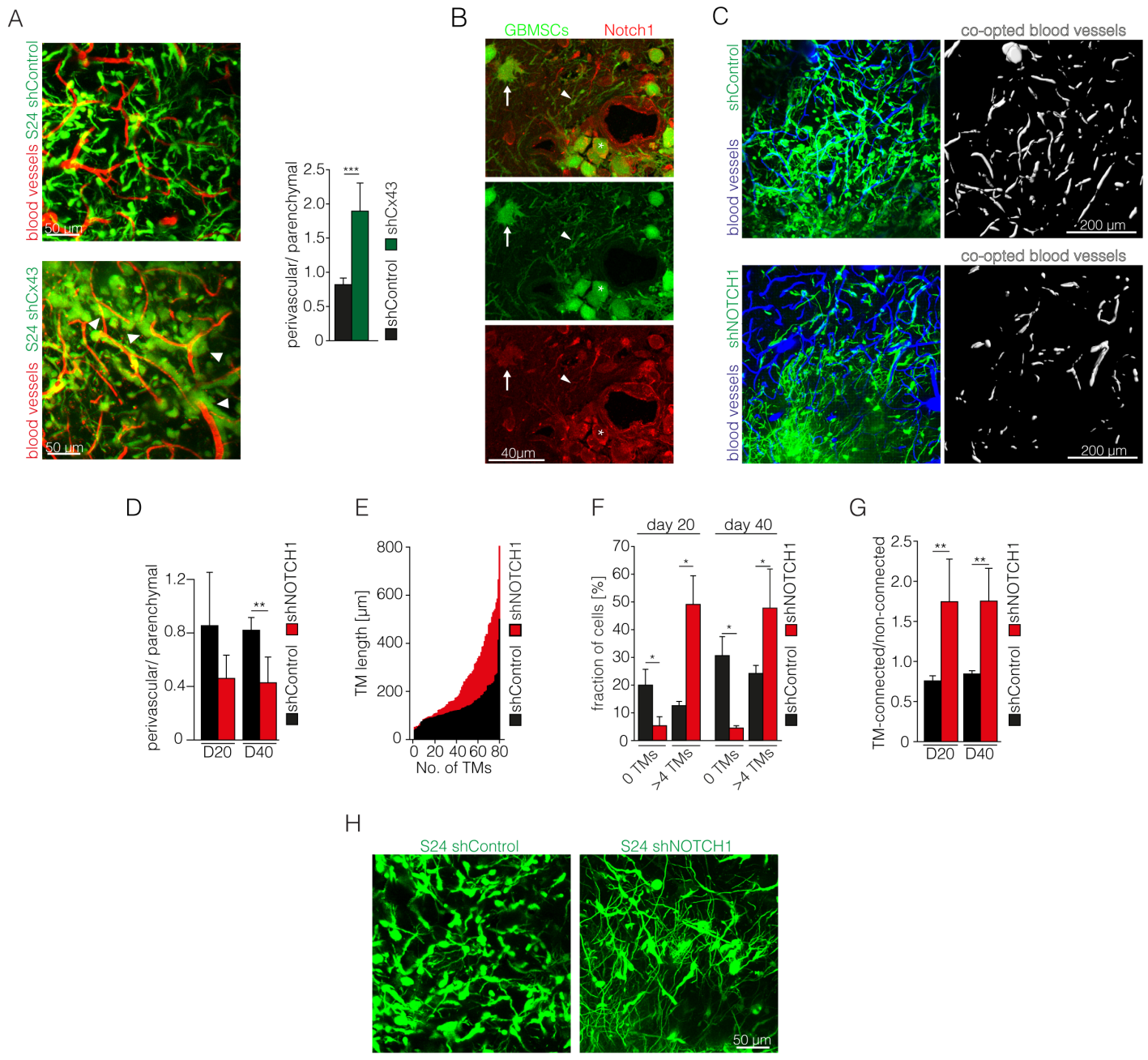

Figure 5

Figure 5

NOTCH1 inhibition leads to depletion of the perivascular niche but promotes TM-network formation (A) Left: Exemplary in vivo 2-PM images of S24 shControl (left, D40) and shCX43 tumors (right, D43). Right: Corresponding Ratio of perivascular and parenchymal cells in S24 shControl and shCX43 knockdown tumors (D40+/-4, n=3 animals per group, t-test). (B) Immunofluorescence staining of activated Notch1 in a S24 tumor section. Arrow: multi-TM parenchymal cell (low Notch1 activation); arrow head: Notch1-low TM; asterisk: perivascular cell (high Notch1 activation). (C) Exemplary 2-PM images of S24 shControl

(top) and shNOTCH1 (bottom) GBMSCs (green) with segmentation of co-opted blood vessels (white) demonstrating a reduced population of the perivascular compartment after NOTCH1 downregulation (D24 ± 1). Blood vessels (blue). (D) Ratio of the perivascular and parenchymal cell count 20 and 40 days after S24 shControl and shNOTCH1 tumor cell implantation (n=3-4 mice per group, 38-445 cells, t-tests). (E) Histogram and quantification of TM length in S24 shControl and shNOTCH1 GBSMSCs (D20, n=3-4 mice per group). (F) Quantification of TM-devoid (0 TMs) vs. TM-rich (> 4 TMs) S24 shControl and shNOTCH1 GBMSCs (n=3-4 mice per group, 18-286 cells, ANOVA on the ranks). (G) Ratio of connected and unconnected S24 shControl and shNOTCH1 GBMSCs 20 and 40 days after tumor cell implantation (n=3-4 mice per group, 11-245 cells, Mann-Whitney tests). (H) Corresponding 2-PM images demonstrating the TM richness of S24 shNOTCH1 tumors (D40). Data (A,D,F,G) are represented as mean ± SD.

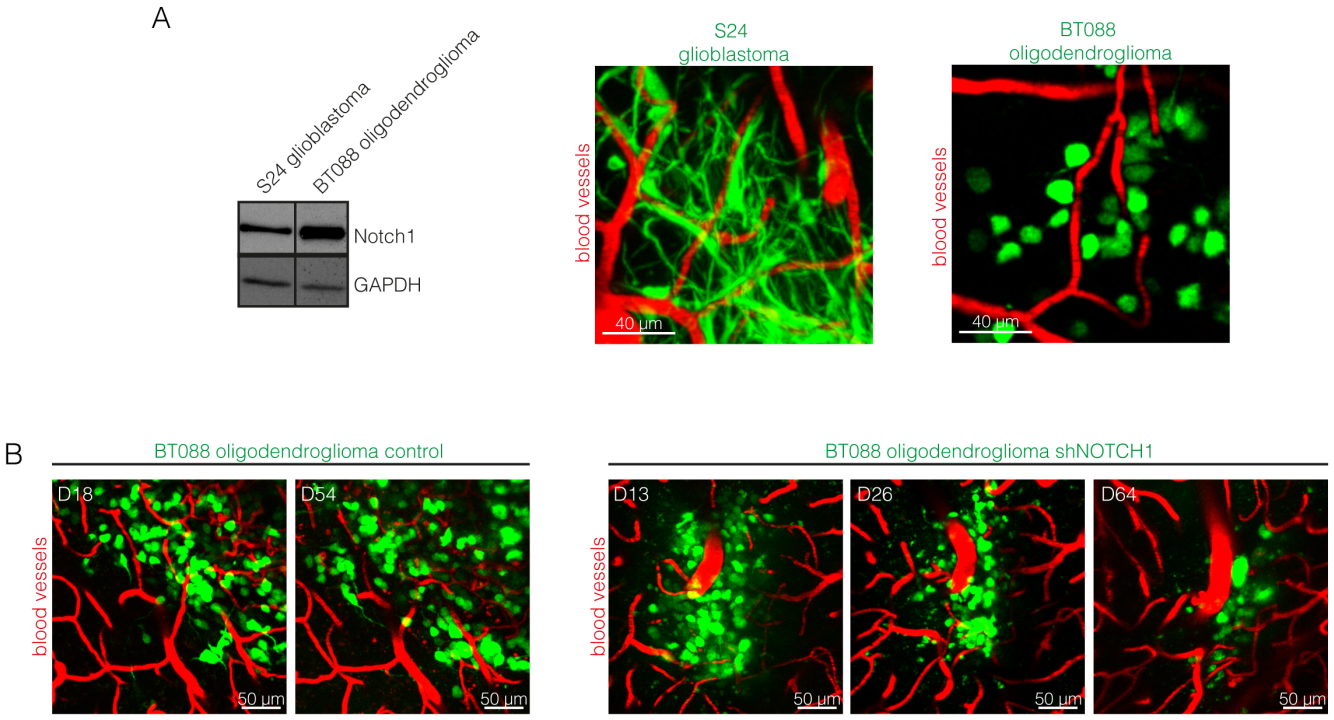

Figure 6

Figure 6

TM-deficient oligodendrogliomas depend on NOTCH1 pathway activation (A) Left: Western blot analysis of the Notch1 expression in S24 GBMSCs and BT088 oligodendroglioma cells. Loading control: GAPDH. Right: Exemplary intravital 2-PM images of S24 glioblastoma and BT088 oligodendroglioma cells (D21 after tumor implantation). (B) Exemplary images of BT088 shControl oligodendroglioma cells and BT088 shNOTCH1 cells demonstrate tumor regression after NOTCH1 knockdown.

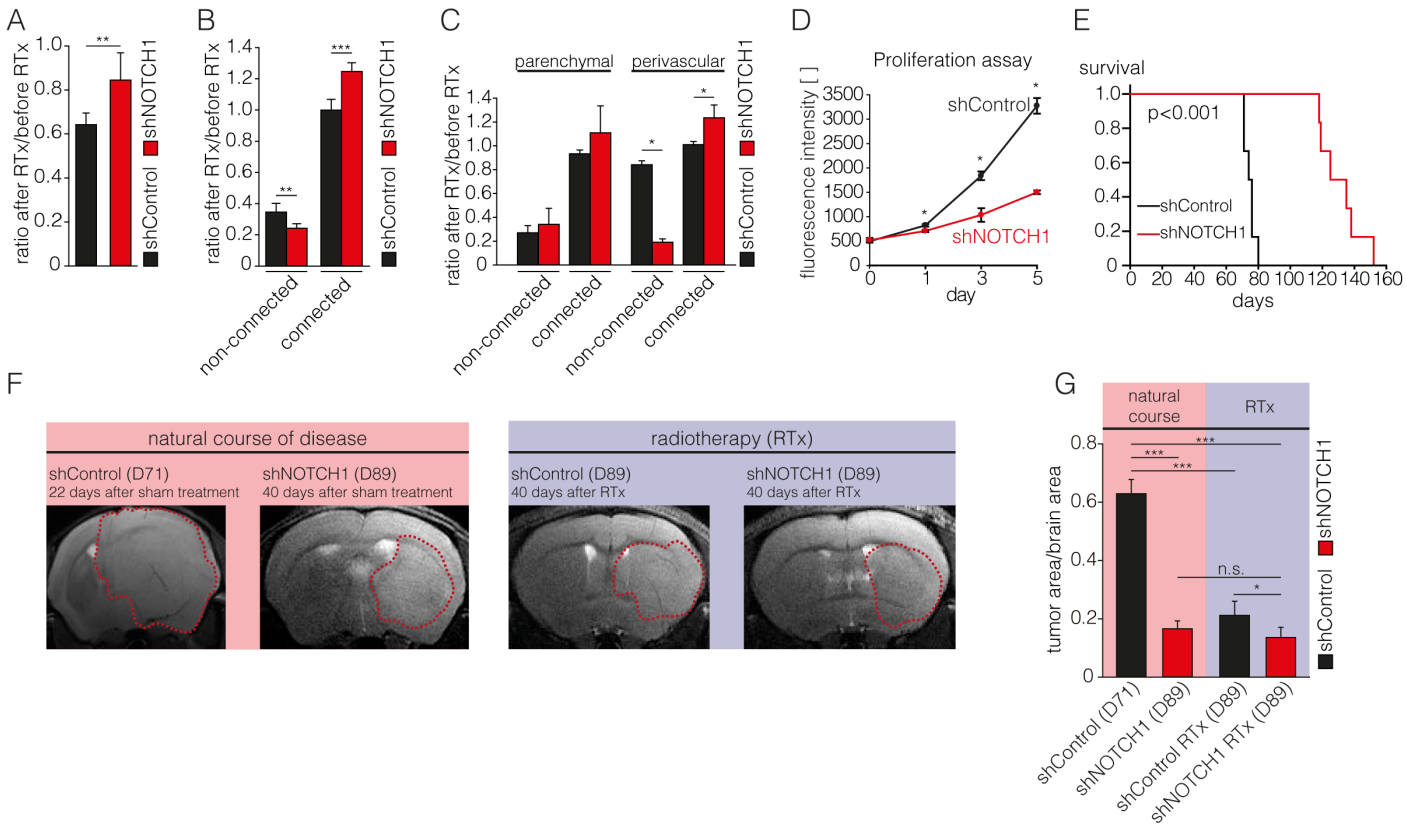

Figure 7

Figure 7

NOTCH1 downregulation sensitizes perivascular glioma cells to radiotherapy, but induces network resistance (A, B) Ratio of cell counts 7 days after and before irradiation of S24 shControl and shNOTCH1 tumors (n=3 mice per group, t-tests). (C) Subgroup analysis of the ratio of cell counts of S24 shControl and shNOTCH1 cells 7 days after and before irradiation categorized regarding connectivity and compartment (n=3 mice per group, t-tests). (D) AlamarBlue proliferation assay of S24 shControl and shNOTCH1 cells (n=6 replicates, ANOVA on ranks). (E) Survival analysis of S24 shControl and shNOTCH1 tumor bearing mice (n=6 mice per group, log rank test). (F) Exemplary 9.4T MRI images of S24 shControl and shNOTCH1 tumors. Left: natural course, right: 40 days after irradiation (RTx). (G) Quantification of tumor burden (tumor area/brain area on 9.4T MRI) in untreated and irradiated mice (n=6 mice per group, ANOVA). Data (A-D,G) are represented as mean ± SD.

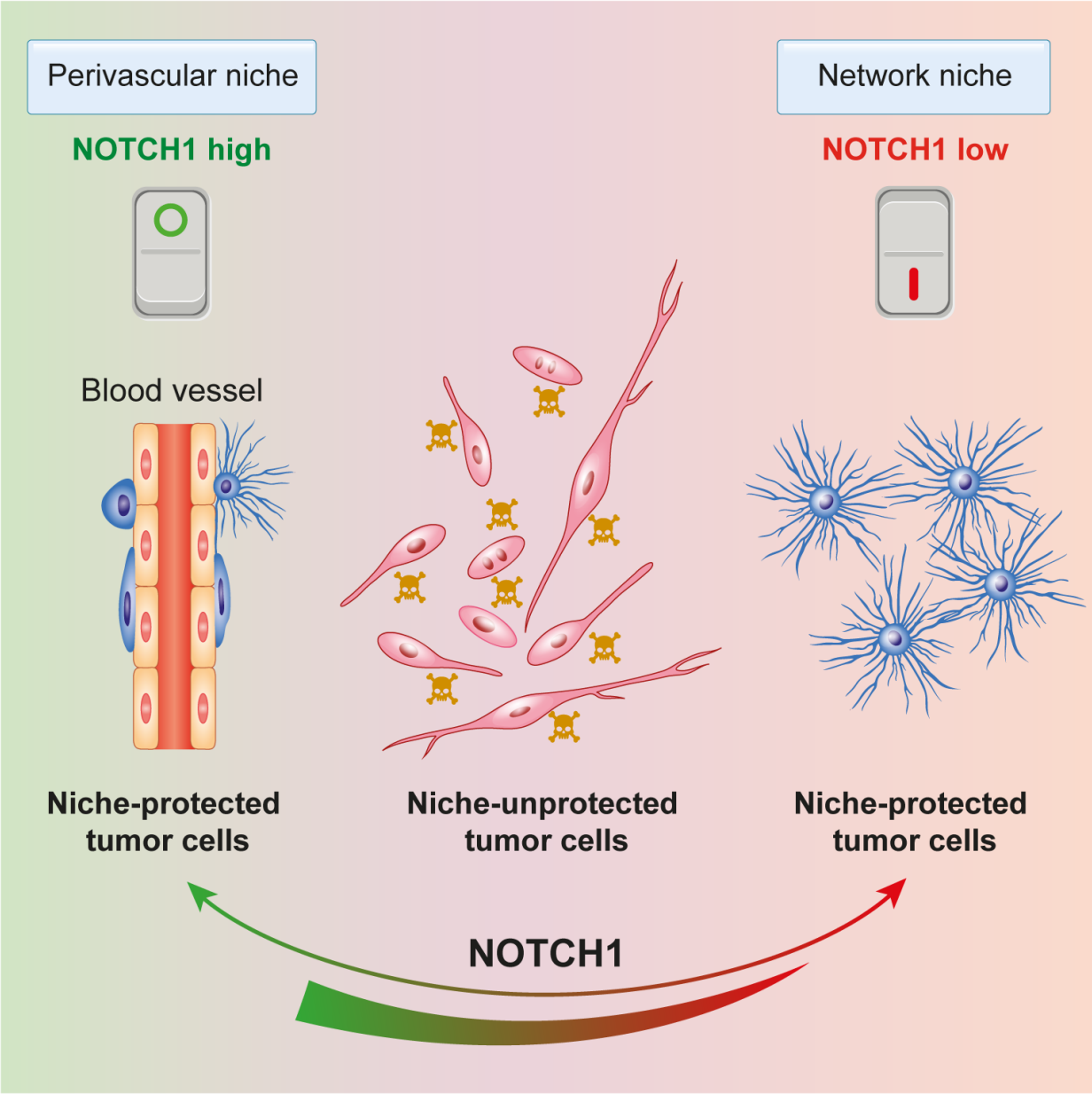

Figure 8

Figure 8

NOTCH1 acts as a switch between the PVN and the network niche Graphical abstract of the two niches of resistance in glioblastoma. The perivascular niche (PVN) (left) is sustained by the NOTCH1 pathway, whereas low NOTCH1 expression leads to depletion of the perivascular niche and the induction of resistant multicellular networks (right). Non-connected, parenchymal cells (middle) in contrast are sensitive to cytotoxic therapies.